Journal of Materials Science and Chemical Engineering, 2020, 8, 1-11
https://www.scirp.org/journal/msce
ISSN Online: 2327-6053
ISSN Print: 2327-6045

Some Optical, Electrical Properties of Lead Free KNN-CZN Ceramics

Phan Dinh Gio*, Truong Thanh Bau, Ngo Vu Hoai, Nguyen Quoc Nam

Department of Physics, University of Sciences, Hue University, Hue, Vietnam
Email: *pdg_55@yahoo.com

How to cite this paper: Gio, P.D., Bau, T.T., Hoai, N.V. and Nam, N.Q. (2020) Some Optical, Electrical Properties of Lead Free KNN-CZN Ceramics. *Journal of Materials Science and Chemical Engineering*, **8**, 1-11.
https://doi.org/10.4236/msce.2020.87001

Received: June 15, 2020
Accepted: July 12, 2020
Published: July 15, 2020

Abstract

Lead free $(1-x)K_{0.5}Na_{0.5}NbO_3$-$xCa(Zn_{1/3}Nb_{2/3})O_3$ (abbreviated KNN-xCZN) ferroelectric ceramics, with x = 0, 0.02, 0.04, 0.06, 0.08, 0.10, have been fabricated by the conventional solid-state reaction method. The effects of CZN content on the structure, microstructure and some optical, electrical properties of KNN-xCZN ceramics were studied in detail. The experimental results showed that the crystal structure of ceramics gradually transformed from orthorhombic phase into pseudo-cubic phase with doping of $xCa(Zn_{1/3}Nb_{2/3})O_3$. With increasing of the CZN concentration, the ceramic density increased and reached the highest value (4.29 g/cm^3) at x = 0.08 mol, besides, the grain size of the ceramics decreased gradually, the microstructure more uniform, the grains are packed with clear grain boundaries, fewer pores, especially at x = 0.08 mol. With the dense and fine-grained microstructures, the optical transmission of the ceramics is strong, the ceramic sample with x = 0.08 mol exhibits stably high transmittance above 60% in the visible spectrum and the largest optical band gap energy (E_g = 3.0 eV) was obtained. The Curie temperature (T_C) decreases when the concentration of CZN increases. The broadness of dielectric peaks around T_m indicated a diffusive phase transition for all compositions suggesting the relaxor-like behavior of KNN-xCZN ceramic systems.

Keywords

Microstructure, Optical Property, Dielectric, Ferroelectric, KNN-xCZN

1. Introduction

Due to environmental pollution caused by lead-containing materials, lead-free piezoceramics have attracted more and more researchers. In recent years, many various lead-free ceramic systems with perovskite structure have been success-

fully studied [1] [2] [3] [4] [5], among which (Na,K)NbO_3 (KNN) based ceramics have attracted a lot of attention due to their strong ferroelectricity, high Curie temperature (about 420˚C). With compositional modification by combining KNN with other perovskite compounds to form KNN-based new solid solutions, such as KNNL [6] [7], KNNLS [8], KNNLST [9], KNNS-BNKZ [10], KNNS-BKZZ [11], the piezoelectric properties of ceramics are further enhanced (d_{33} > 400 pC/N) [12] [13] [14], thereby it has become one of the most promising candidates for replacing Pb-based ceramics in the piezoelectric field. However, most of these studies focused on electrical properties, while the optical properties of the material are rarely mentioned.

As known, lead-free transparent ferroelectric ceramics is a new type of functional material which is friendly to environment, they have great potential in the fields of optoelectronics, infrared detection, lasers and optical storage [15]. Transparent ceramics have been studied since the 1970s on the basis of lead-containing materials such as PLZT [16], PMN-PT [17]. However, due to the toxicity of lead, current studies are focusing on lead-free transparent ferroelectric ceramic materials based on KNN [18], BNKT [19].

This paper presents some research results on structure, microstructure and optical, electrical properties of the lead-free $(1-x)K_{0.5}Na_{0.5}NbO_3$-$xCa(Zn_{1/3}Nb_{2/3})O_3$ ceramics.

2. Experimental Procedure

The $(1-x)K_{0.5}Na_{0.5}NbO_3$-$xCa(Zn_{1/3}Nb_{2/3})O_3$ (abbreviated KNN-xCZN) ferroelectric ceramics, with x = 0, 0.02, 0.04, 0.06, 0.08 and 0.1 were synthesized by a conventional mixed-oxide method. The carbonates K_2CO_3, Na_2CO_3, $CaCO_3$ and oxides Nb_2O_5, ZnO (purity ≥ 99%) were used as starting materials. Before being weighed, the K_2CO_3 and Na_2CO_3 powders were dried in an oven at 150˚C for 2 hours to minimize the effect of moisture. Mixed powder was milled for 8 hours with the ZrO_2 balls in ethanol. The powders were calcined at temperature of 850˚C for 2 hours to obtain the KNN-CZN compound. Thereafter the calcined powders were ball milled again for 18 hours. The ground materials were pressed into disk 12 mm in diameter and 1.5 mm in thick under 1.5 T/cm^2 and then were sintered at temperature of 1130˚C for 2 hours.

The crystal structure of the ceramic specimens was examined by X-ray diffraction (XRD, D8 ADVANCE) with CuK_α radiation of wavelength 1.5405 Å at room temperature. The microstructure of the specimens was examined by using a scanning electron microscope (SEM) (Hitachi S-4800). The density of specimens was measured by Archimedes method. To measure electrical properties, the ceramic specimens were coated with silver paint on two surfaces and heated at 600˚C for 15 min. Temperature dependence of dielectric constant and dielectric loss were determined using RLC HIOKI 3532 with automatic programming. The ferroelectric properties were measured by Sawyer-Tower method. The optical transmission spectrum from 200 to 900 nm was measured by using ultraviolet-visible-near infrared spectroscopy (Genesys 10S UV-Vis (Thermo Scien-

tific)), the specimens were polished to 0.5 mm thickness.

3. Results and Discussion

3.1. Structure and Microstructure

Figure 1(a) shows the XRD patterns were measured in the range of 2θ from 20˚ to 80˚ of the KNN-xCZN ceramic specimens sintered at temperature of 1130˚C for 2 hours. It can be seen that all the ceramics exhibit the coexistence of perovskite phase, no secondary phase was detected. This means that CZN has diffused into the KNN lattice and formed a homogeneous solid solution, in which Zn^{2+} (0.74 Å) replaced site of Nb^{5+} (0.64 Å) in the octahedral center, and the replacement of K^{+} (1.64 Å) and Na^{+} (1.39 Å) by Ca^{2+} (1.34) due to the similarity of the ionic radius [20].

To further determine the effect of CZN doping on the crystalline phase transition of KNN-xCZN ceramics, the X-ray diffraction patterns at $2\theta \approx 45.5^{\circ}$ of all specimens have been enlarged and simulated using the Gauss fitting function (Figure 1(b)). The simulated data confirm that phase structure of ceramic specimens with $x \leq 0.04$ was orthorhombic perovskite ABO_3 type similar to pure KNN ceramics at room temperature, which is characterized by the double peaks (220) and (020) with a relative intensity ratio of $I_{220}/I_{002} = 2/1$ [21]. At $x = 0.06$, the ceramics showed a mixed orthorhombic and pseudo-cubic phase. As x further increases ($x > 0.06$), the ceramics should be a pseudo-cubic phase as characterized by the single peak (200) at $2\theta \approx 45.5^{\circ}$. These results are similar to the work of Qizhen Chai *et al.* [22]. According to the published works [18] [23], the ceramics of symmetrical pseudo-cubic phase generally have the lowest anisotropy, which leads to a decrease in light scattering at the grain boundaries and an increase in optical transmittance.

Table 1 shows density, dielectric constant (ε_r), dielectric loss ($\tan\delta$) at the room temperature, Curie temperature (T_C) and the average grain size of KNN-xCZN ceramics as a function of the CZN content. As shown, the bulk

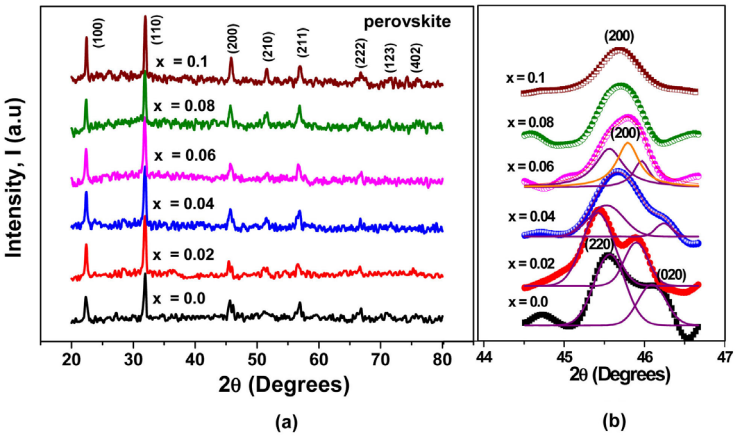

Figure 1. (a) XRD patterns of the $(1 - x)K_{0.5}Na_{0.5}NbO_3$-$xCa(Zn_{1/3}Nb_{2/3})O_3$ ceramics with $x = 0$, 0.02, 0.04, 0.06, 0.08 and 0.1; (b) Expanded XRD patterns of the ceramic spcimens at $2\theta \approx 45.5^{\circ}$ and simulated using the Gauss function.

Table 1. Relative density (D), dielectric constant (ε_r), dielectric loss (tanδ), Curie temperature (T_C) and mean grain size of the KNN-xCZN ceramics.

x content (mol)	D (g/cm^3)	ε_r	tanδ	T_C (˚C)	Mean grain size (μm)
0.0	3.64	434	0.062	286	3.0
0.02	3.82	604	0.047	285	2.5
0.04	3.84	960	0.042	234	1.7
0.06	4.06	1135	0.032	199	0.8
0.08	4.29	1334	0.01	149	0.4
0.1	4.10	1463	0.02	108	1.5

density increased with increasing of x content and reached the highest value (4.29 g/cm^3) at x = 0.08 mol, then decreased, indicating that with the concentration x of 0.08 mol, the density of KNN-xCZN ceramics is the best. This result is consistent with the microstructure of fracture surfaces of the KNN-xCZN ceramics as shown in **Figure 2**. From **Table 1**, it can be seen that when the concentration of CZN increases, the room temperature dielectric constant (ε_r) and dielectric loss (tanδ) measured at 10 kHz of KNN-xCZN ceramics increased and decreased, respectively. This is explained that the replacement of K^+ (1.64 Å) and Na^+ (1.39 Å) are occupying the A sites of the perovskite lattice by Ca^{2+} (1.34 Å) will cause formation of K^+ and Na^+ ion vacancies. When two A sites are occupied by two cations with a valence of +2, a Na (K) vacancy is created in the lattice to maintain electroneutrality. This result may contribute to the mobility of domain walls, and the dielectric constant is increased and dielectric loss decreased [24].

Figure 2 shows SEM patterns of the fracture surfaces for the KNN-xCZN ceramic specimens sintered at 1130˚C.

As shown in **Figure 2**, all the ceramic specimens show cubic-like grains, it is characteristic shape of KNN-based materials. The concentration of CZN has strongly influenced on the microstructure of KNN-xCZN ceramics, with increasing of CZN doping, the average grain size of ceramics has decreased significantly. The undoped ceramic specimen (x = 0) had a porous microstructure, the distribution of discrete grains, corresponding to low density (3.64 g/cm^3), the average size of the grains is abnormally large, 3.0 μm. However, as seen in **Table 1** and **Figure 2**, when doped CZN with x ≤ 0.06, the microstructure of ceramics is gradually improved, the average grain size decreased from 2.5 μm to 0.8 μm, the relatively more uniform grains with cubic shapes; however, there are still some porous holes, maybe this is the reason for low density (≤4.06 g/cm^3). Further increasing the CZN content to 0.08 mol, the average grain size of the ceramics decreased to a lowest value (0.4 μm), amount of porous decreased markedly, the microstructure of ceramics becomes denser, corresponding to highest density (4.29 g/cm^3). Microstructures with fine grains are an important factor that reduces light scattering and increases the transmittance of the ceramics [23]. When the amount of CZN increases to 0.1 mol, the average grain size of ceramics increases (1.5 μm), and porous microstructure.

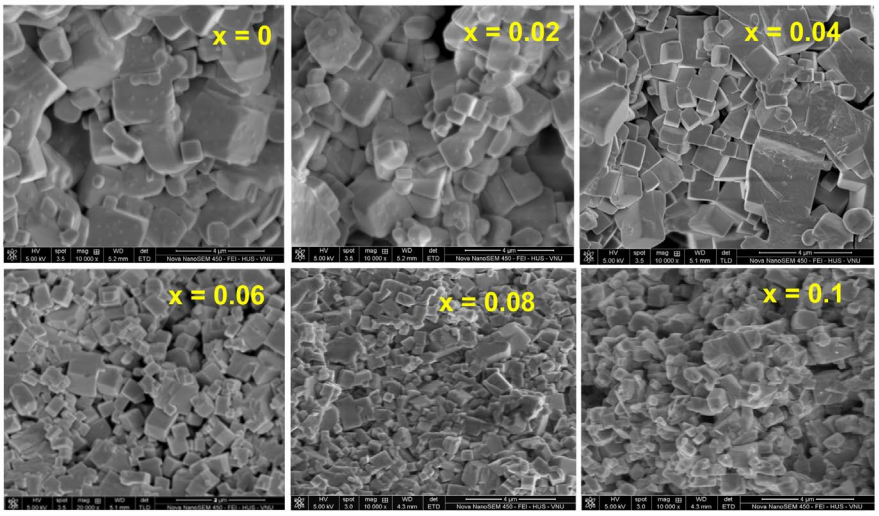

Figure 2. SEM micrographs of KNN-xCZN ceramic specimens with $x = 0.0$, $x = 0.02$, $x = 0.04$, $x = 0.06$, $x = 0.08$ and $x = 0.1$.

3.2. Optical Properties

Figure 3 shows the optical transmittances (T) of the KNN-xCZN ceramic specimens measured in the range of 200 - 900 nm.

As seen from **Figure 3**, in the measured wavelength region, the transmittance increases with increasing x from 0 to 0.08 and then decreases when $x = 0.1$. The ceramic specimen with x = 0.08 exhibits high transmittance above 60% in the visible spectra. For further research of the optical transmission of ceramics, the CZN concentration dependence of optical transmittance of KNN-xCZN for light at wavelength 680 nm shown in **Figure 4**. The transmittance increases sharply with increasing of x concentration, reaches a maximum value of 62% at x = 0.08 and then decreases. The high transparency of ceramic specimen with concentration x of 0.08 may be due to fine grain size (400 nm), low porosity, high crystal structure symmetry (discussed in the previous section) and relaxor behavior (will be mentioned in a later section).

The value of optical band gap energy (E_g) is very important for studies of optical characteristics, which can be calculated from the absorption spectrum using the Tauc equation [25]. For direct transition, the relationship between E_g, photon frequency ν and the absorption coefficient α is given as:

$$(\alpha h\nu)^2 = A(h\nu - E_g) \tag{1}$$

where h is Planck's constant (4.1357×10^{-15} eV) and A is a constant. The absorption coefficient α is calculated by the formula:

$$\alpha = \frac{1}{t}\ln\left(\frac{1}{T}\right) \tag{2}$$

t is the thickness of the sample, T is the transmittance.

The optical band gap energy (E_g) is calculated by plotting $(\alpha h\nu)^2$ versus $h\nu$ and extrapolating the linear portion of the curve to zero, as shown in **Figure 5**.

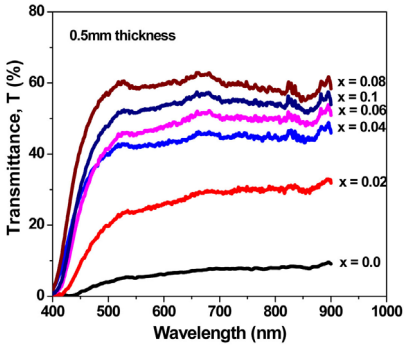

Figure 3. Optical transmittance spectra of the KNN-xCZN transparent ceramics.

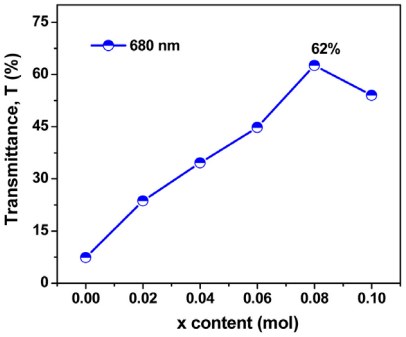

Figure 4. CZN concentration dependence of optical transmittance of KNN-xCZN ceramics measured at wavelength 680 nm.

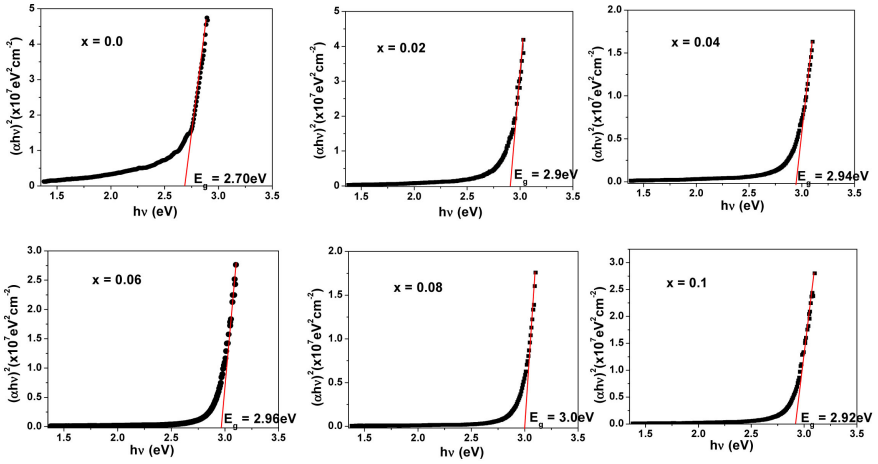

Figure 5. Plot of $(ah\nu)^2$ versus $h\nu$ and the values of E_g for the KNN-xCZN transparent ceramics at the different concentrations of CZN.

From the results in **Figure 5**, x content dependence of E_g of KNN-xCZN ceramics shown in **Figure 6**. As seen, with increasing x from 0 to 0.08 mol, the E_g band gap energy increases from 2.7 eV at x = 0 to a maximum value of 3.0 eV at x = 0.08, then decreased, indicating that the doping of CZN has a great influence on the band gap energy of the KNN-xCZN ceramics. Thus, it is obvious that the value of E_g is closely related to optical transmission, materials with large E_g values will have high optical transparency [22].

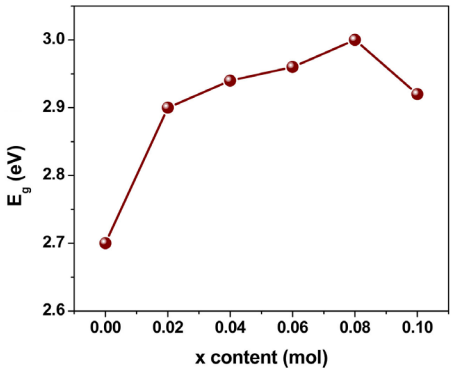

Figure 6. The values of band gap energy E_g of KNN-xCZN ceramics at the different x content.

3.3. Electrical Properties

Figure 7 shows the temperature dependence of dielectric constant ε_r, and dielectric loss $\tan\delta$ measured at 10 kHz frequency in the temperature range of 28˚C - 320˚C of KNN-xCZN ceramics sintered at 1130˚C. As seen, the (ε-T) curves of the ceramic samples with x = 0, 0.02, 0.04 and 0.06 have two obvious peaks: a peak at low temperature, which is the peak corresponding to the ferroelectric phase transition temperatures $T_{O\text{-}T}$, however, when x > 0.06, the $T_{O\text{-}T}$ peak is suppressed. The second peak at higher temperatures, corresponding to the ferroelectric-paraelectric phase transition temperature (the T_C Curie temperature). While only one dielectric peak (T_C) is observed in the ceramics with x = 0.08 - 0.1. The T_C is significantly dependent on the CZN content and gradually decreases from 285˚C to 110˚C as the x content of CZN increases (the inset **Figure 7**), this result is related to the structural change of ceramics when the concentration of CZN increases as discussed above. In addition, the results also show that with increasing of x content from 0 to 0.02, the dielectric peaks of ceramics are still sharp, indicating that the ceramics are a normal ferroelectrics [24], however, when $x \geq 0.04$, the shape of the dielectric peaks became broaden, exhibit the diffuse phase transition, it is one of the characteristics for the relaxor ferroelectrics [24]. Besides, the dielectric loss $\tan\delta$ decreases as the temperature rises from room temperature to 200˚C, and after that the value of $\tan\delta$ increases sharply related to the increased conductivity at high temperature [26].

For the relaxor ferroelectrics, when $T > T_m$ (mean value of T_C), the relationship between dielectric constant and temperature obey the Uchino function [27]:

$$\frac{1}{\varepsilon} - \frac{1}{\varepsilon_{\max}} = \frac{(T - T_m)^{\gamma}}{C} \tag{3}$$

where, $\varepsilon_{\max}$ is the maximum value of dielectric constant at the phase transition temperature T_m, C is the Curie-like constant and γ is a diffusion coefficient, with γ = 1: normal ferroelectrics, 1 < γ < 2: relaxor-like ferroelectrics, γ = 2: ideal relaxor ferroelectrics. The plot of $\ln(1/\varepsilon - 1/\varepsilon_{\max})$ versus $\ln(T - T_m)$ of KNN-xCZN ceramics with x from 0.04 to 0.1 shown in **Figure 8**. The results show that these

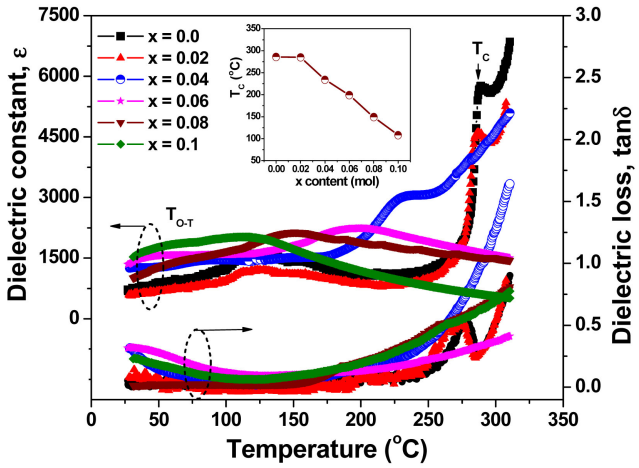

Figure 7. Temperature dependence of dielectric constant ε and dielectric loss tanδ (10 kHz) of the KNN-xCZN ceramics measured at 10 kHz. The inset is plot of T_C versus x content.

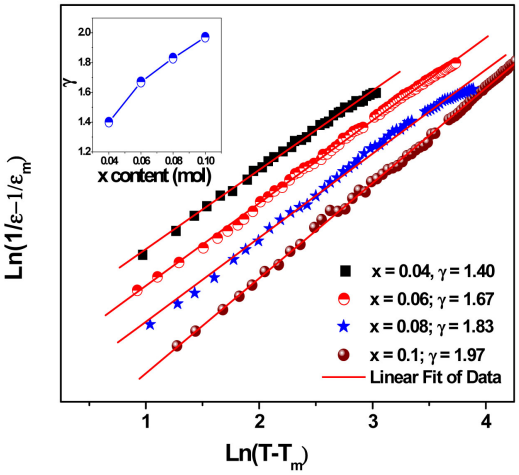

Figure 8. $\ln(1/\varepsilon - 1/\varepsilon_m)$ as a function of $\ln(T - T_m)$ for the KNN-xCZN ceramics.

relationships are linear. The slopes of the fitting curves are used to determine the γ values. The values of γ increased from 1.4 to 1.97 when x content increases from 0.04 to 0.1, indicating transitions are of diffuse type, which is one of the most important characteristics of relaxor ferroelectrics.

Figure 9 shows the shape of the ferroelectric hysteresis loops of the KNN-xCZN ceramic specimens measured at room temperature. As seen, the shape of loop becomes slimmer with increasing of CZN content especially for compositions with $x > 0.06$. From the shape of these loops, the remanent polarization (P_r) and the coercive field (E_C) were determined. As shown in Figure 10, with increasing of CZN content from 0 to 0.1 mol, a sharp decrease in P_r from 11.4 to 3.3 μC/cm^2 were observed for ceramics, indicating that the ferroelectric properties are strongly reduced due to the increase of the crystal symmetry from orthorhombic to pseudo-cubic caused by relaxor behavior. Similarly the coercive field E_C strong decreased from 9.65 to 5.5 kV/cm.

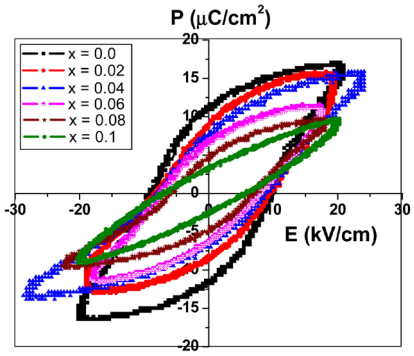

Figure 9. Hysteresis loops of KNN-xCZN ceramics measured at room temperature.

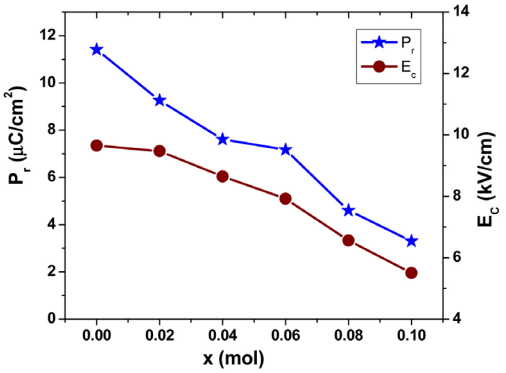

Figure 10. The remnant polarization (P_r) and coercive field (E_C) of KNN-xCZN ceramics as a function of the CZN content.

4. Conclusion

The $(1-x)K_{0.5}Na_{0.5}NbO_3$–$xCa(Zn_{1/3}Nb_{2/3})O_3$ (x = 0, 0.02, 0.04, 0.06, 0.08 and 0.1) lead-free ferroelectric ceramics were successfully fabricated by conventional sintering method. The effect of CZN addition on the structural phase transition, microstructure and dielectric, ferroelectric properties of ceramics were investigated in detail. The addition of CZN caused an increase in the density and decrease in grain size of ceramics. All samples have perovskite phase structure with a change from orthorhombic (x ≤ 0.04) to the orthorhombic-pseudocubic mixed phases at x = 0.06 and finally the pseudo-cubic phase structure when $x \geq 0.08$. With the dense and fine-grained microstructures, the optical transmission of the ceramics is strong, at x = 0.08 mol the ceramic exhibits stably high transmittance above 60% in the visible spectrum and the largest optical band gap energy (E_g = 3.0 eV). The Curie temperature decreased gradually and the shape of the dielectric peaks became broaden with $x \geq 0.04$ indicating a diffusive phase transition for compositions suggesting the relaxor-like behavior of KNN-xCZN ceramic systems.

Acknowledgements

This research is funded by Vietnam National Foundation for Science and Technology Development (NAFOSTED) under grant number 103.02-2019.08.

Conflicts of Interest

The authors declare no conflicts of interest regarding the publication of this paper.

References

[1] Zuo, R.Z., Su, S., Wu, Y., Fu, J., Wang, M. and Li, L.T. (2008) Influence of A-Site Nonstoichiometry on Sintering, Microstructure and Electrical Properties of $(Bi_{0.5}Na_{0.5})TiO_3$ Ceramics. *Materials Chemistry and Physics*, **110**, 311-315. https://doi.org/10.1016/j.matchemphys.2008.02.007

[2] Bhandari, S., Sinha, N., Raya, G. and Kumar, B. (2014) Processing and Properties of Ferroelectric $Bi_{0.5}(Na_{0.65}K_{0.35})_{0.5}TiO_3$ Ceramics under the Effect of Different Sintering Temperature. *Scripta Materialia*, **89**, 61-64. https://doi.org/10.1016/j.scriptamat.2014.06.029

[3] Wang, K. and Li, J.-F. (2012) $(K,Na)NbO_3$-Based Lead-Free Piezoceramics: Phase Transition, Sintering and Property Enhancement. *Journal of Advanced Ceramics*, **1**, 24-37. https://doi.org/10.1007/s40145-012-0003-3

[4] Gio, P.D., Viet, H.Q. and Vuong, L.D. (2018) Low-Temperature Sintering of $0.96(K_{0.5}Na_{0.5})NbO_3$-$0.04LiNbO_3$ Lead-Free Piezoelectric Ceramics Modified with CuO. *International Journal of Materials Research*, **109**, 1071-1076. https://doi.org/10.1166/asem.2019.2364

[5] Karaki, T., Yan, K., Miyamoto, T. and Adachi, M. (2007) Lead-Free Piezoelectric Ceramics with Large Dielectric and Piezoelectric Constants Manufactured from $BaTiO_3$ Nano-Powder. *Japanese Journal of Applied Physics*, **46**, L97-L98. https://doi.org/10.1143/JJAP.46.L97

[6] Gio, P.D. and Lien, N.T.K. (2015) Effect of $LiNbO_3$ on the Structure, Microstructure and Dielectric, Ferroelectric Properties of $(K_{0.5}Na_{0.5})NbO_3$ Lead Free Ceramics. *Indian Journal of Scientific Research and Technology*, **3**, 48-53.

[7] Matsubara, M., Kikuta, K. and Hirano, S. (2005) Piezoelectric Properties of $(K_{0.5}Na_{0.5})(Nb_{1-x}Ta_x)O_3$-$K_{5.4}CuTa_{10}O_{29}$ Ceramics. *Journal of Applied Physics*, **97**, Article ID: 114105. https://doi.org/10.1063/1.1926396

[8] Li, H.D., *et al*. (2007) Effect of Antimony Concentration on the Crystalline Structure, Dielectric, and Piezoelectric Properties of $(Na_{0.5}K_{0.5})_{0.945}Li_{0.055}Nb_{1-x}Sb_xO_3$ Solid Solutions. *Journal of the American Ceramic Society*, **90**, 3070-3072. https://doi.org/10.1111/j.1551-2916.2007.01875.x

[9] Gio, P.D. and Phong, N.D. (2015) Effects of LiF on the Structure and Electrical Properties of $(Na_{0.52}K_{0.435}Li_{0.045})Nb_{0.87}Sb_{0.08}Ta_{0.05}O_3$ Lead-Free Piezoelectric Ceramics Sintered at Low Temperatures. *Journal of Materials Science and Chemical Engineering*, **3**, 13-20. https://doi.org/10.4236/msce.2015.311003

[10] Tangsritrakul, J. and Hall, D.A. (2017) Structural and Functional Characterisation of KNNS-BNKZ Lead-Free Piezoceramics. *Advances in Applied Ceramics*, **117**, 42-48. https://doi.org/10.1080/17436753.2017.1366733

[11] Wu, J.G. and Wang, Y.M. (2014) Two-Step Sintering of New Potassium Sodium Niobate Ceramics: A High d33 and Wide Sintering Temperature Range. *Dalton Transactions*, **43**, 12836-12841. https://doi.org/10.1039/C4DT01712A

[12] Wang, X.P., Wu, J.G., Xiao, D.Q., Zhu, J.G., Cheng, X.J., Zheng, T., Zhang, B.Y., Lou, X.J. and Wang, X.J. (2014) Giant Piezoelectricity in Potassium-Sodium Niobate Lead-Free Ceramics. *Journal of the American Chemical Society*, **136**, 2905-2910. https://doi.org/10.1021/ja500076h

[13] Cheng, X.J., Wu, J.G., Wang, X.P., Zhang, B.Y., Zhu, J.G., Xiao, D.Q., Wang, X.J., and Lou, X.J. (2013) Giant d33 in $(K,Na)(Nb,Sb)O_3$-$(Bi,Na,K,Li)ZrO_3$ Based Lead-Free

Piezoelectrics with High T_C. *Applied Physics Letters*, **103**, Article ID: 052906. https://doi.org/10.1063/1.4817517

[14] Saito, Y., Takao, H., Tani, T., Nonoyama, T., Takatori, K., Homma, Nagoya, T. and Nakamura, M. (2004) Lead-Free Piezoceramics. *Nature*, **432**, 84-87. https://doi.org/10.1038/nature03028

[15] Geng, Z.M., Li, K., Shi, D.L., Zhang, L.L. and Shi, X.Y. (2015) Effect of Sr and Ba-Doping in Optical and Electrical Properties of KNN Based Transparent Ceramics. *Journal of Materials Science*: *Materials in Electronics*, **26**, 6769-6775. https://doi.org/10.1007/s10854-015-3287-6

[16] Haertling, G.H. (1999) Ferroelectric Ceramics: History and Technology. *Journal of the American Ceramic Society*, **82**, 797-818. https://doi.org/10.1111/j.1151-2916.1999.tb01840.x

[17] Fujii, I., Yoshida, R., Imai, T., Yamazoe, S. and Wada, T. (2013) Fabrication of Transparent $Pb(Mg_{1/3}Nb_{2/3})O_3$-$PbTiO_3$ Based Ceramics by Conventional Sintering. *Journal of the European Ceramic Society*, **96**, 3782-3787. https://doi.org/10.1111/jace.12574

[18] Chai, Q.Z., Yang, D., Zhao, X.M., Chao, X.L. and Yang, Z.P. (2018) Lead-Free (K,Na)NbO_3-Based Ceramics with High Optical Transparency and Large Energy Storage Ability. *Journal of the American Ceramic Society*, **101**, 2321-2329. https://doi.org/10.1111/jace.15392

[19] Quan, N.D., Quyet, N.V., Bac, L.H., Thiet, D.V., Hung, V.N. and Dung, D.D. (2015) Structural, Ferroelectric, Optical Properties of A-Site-Modified $Bi_{0.5}(Na_{0.78}K_{0.22})_{0.5}Ti_{0.97}Zr_{0.03}O_3$ Lead-Free Piezoceramics. *Journal of Physics and Chemistry of Solids*, **77**, 62-67. https://doi.org/10.1016/j.jpcs.2014.10.010

[20] Yang, D., Ma, C., Yang, Z., Wei, L., Chao, X., Yang, Z. and Yang, J. (2016) Optical and Electrical Properties of Pressureless Sintered Transparent $(K_{0.37}Na_{0.63})NbO_3$-Based Ceramics. *Ceramics International*, **42**, 4648-4657. https://doi.org/10.1016/j.ceramint.2015.11.032

[21] Yao, F.-Z., Patterson, E.A., Wang, K., Jo, W., Rodel, J. and Li, J.-F. (2014) Enhanced Bipolar Fatigue Resistance in $CaZrO_3$-Modified (K,Na)NbO_3 Lead-Free Piezoceramics. *Applied Physics Letters*, **104**, Article ID: 242912. https://doi.org/10.1063/1.4884826

[22] Chai, Q.Z., Zhao, X.M., Chao, X.L. and Yang, Z.P. (2017) Enhanced Transmittance and Piezoelectricity of Transparent $K_{0.5}Na_{0.5}NbO_3$ Ceramics with $Ca(Zn_{1/3}Nb_{2/3})O_3$ Additives. *RSC Advances*, **7**, 28428-28437. https://doi.org/10.1039/C7RA04064D

[23] Zhang, X., Yang, D., Yang, Z., Zhao, X., Chai, Q., Chao, X., Yang, Z., *et al*. (2016) Transparency of $K_{0.5}N_{0.5}NbO_3$-$Sr(Mg_{1/3}Nb_{2/3})O_3$ Lead-Free Ceramics Modulated by Relaxor Behavior and Grain Size. *Ceramics International*, **42**, 17963-17971. https://doi.org/10.1016/j.ceramint.2016.07.069

[24] Xu, Y.H. (1991) Ferroelectric Materials and Their Applications. North-Holland, Amsterdam.

[25] Tauc, J. and Wood, D.L. (1972) Weak Absorption Tails in Amorphous Semiconductors. *Physical Review B*, **5**, 3144-3151. https://doi.org/10.1103/PhysRevB.5.3144

[26] Liu, B.H., Zhang, Y., Li, P., Shen, B. and Zhai, J.W. (2016) Phase Transition and Electrical Properties of $Bi_{0.5}(Na_{0.8}K_{0.2})_{0.5}ZrO_3$ Modified $(K_{0.52}Na_{0.48})(Nb_{0.95}Sb_{0.05})O_3$ Lead-Free Piezoelectric Ceramics. *Ceramics International*, **42**, 13824-13829. https://doi.org/10.1016/j.ceramint.2016.05.186

[27] Uchino, K. (1991) Relaxor Ferroelectrics. *Journal of the Ceramic Society of Japan*, **99**, 829-835. https://doi.org/10.2109/jcersj.99.829